Computer Fraud and Security
ISSN (online): 1873-7056

Bidirectional DC-DC Control Strategy for Photovoltaic Energy Storage based on Fuzzy Second-Order Active Disturbance Rejection

Binjun Cai*, Zhensheng Yao, Zhixiong Liu
School of Electrical and Information Engineering, Hunan institute of Engineering, Xiangtan, Hunan, China
**Corresponding Author.*

Abstract:
A bidirectional DC-DC converter (BDC) control strategy rested on fuzzy second-order linear active disturbance rejection control (FS-LADRC) is proposed to make independent photovoltaic energy storage system (IPESS) better adapt to various external conditions. The linear model of IPESS is constructed. Rested on the control characteristics of BDC on the energy storage side, traditional voltage and current double closed-loop control (VCDCC) is used. PI control is adopted for the current loop, and second-order linear active disturbance rejection control (LADRC) is adopted for the voltage loop. Fuzzy adaptive logic is combined with linear state error feedback (LSEF) control rate, so that the system has higher control accuracy. Compared with traditional PI control and traditional LADRC, the stability of direct current busbar (DCB) voltage and the power generation performance of the system under different conditions are analyzed by changing the intensity of PV irradiance. Simulation results illustrate that FS-LADRC is more excellent to traditional PI and LADRC control strategies in improving the steadiness of DCB voltage, power generation performance and of the system.

Keywords: photovoltaic, energy storage, converters, fuzzy control

INTRODUCTION

With the progress of society, new energy power generation has begun to play a very important role, among which photovoltaic power generation has gradually become a hot spot in the current era, and independent photovoltaic DC microgrid has become a swiftly growing domain in the photovoltaic market [1, 2].Independent photovoltaic power generation is becoming more and more popular with its advantages of flexible operation mode, high energy utilization efficiency, and outstanding environmental protection benefits, but the power supply reliability of this system will be affected by factors such as meteorological environment and load, so the power supply stability is relatively poor, and it is generally required to incorporate energy storage devices (ESD) to enhance the dependability of power supply, and an independent optical storage system is formed. BDC is indispensable in IPESS [3], and its structure and control mode can be related to the power provision reliability of the whole system and the stability of the DCB. While power is being conveyed from the battery to the load, a high voltage gain ratio is needed. Common BDC achieve high voltage gain but with low efficiency, resulting from the high switching stress of operating the semiconductor switch with a large duty cycle. Other than low efficiency and high switching stress level, common BDC bring about electromagnetic interference to neighboring communication systems and possess large ripples in output voltage and current [4, 5]. Therefore, there is potential value in exploring better BDC control methods.

Through theoretical analysis and experimental research, it is found that the BDC control structure in the optical storage system includes VCDCC, I-V droop control and V-P droop control [6]. In this paper, the VCDCC is used as the basic structure of the controller. In recent years, many scholars and experts have made a lot of achievements in order to cope with the challenges faced by IPESS. To address the issues of intermittent power supply from independent power generation and the variation of load power that would result in the instability of bus voltage, a modified super-twist sliding mode control approach based on the super-twist algorithm was put forward.[7]. Proposed a novel multifunctional isolated three-port BDC for stand-alone photovoltaic systems by modifying the structure of the converter [8]. Make the system have a leakage recovery function to improve the conversion efficiency. A new phase-shifting current sharing control strategy was proposed to solve the problems of large inductor current ripple and unbalanced current between two phases that are common in traditional two-phase parallel DC-DC circuits [9]. For the sake of improving the stability of the system and strengthen the resilience to changes in conditions such as voltage disturbance and irradiance change on the DCB side, a nonlinear control

method for non-isolated BDC was proposed, but the design of this controller is not sensitive to system parameters [10].

For the purpose of attaining the stable and efficient running of independent photovoltaic energy storage DC microgrids, the adoption of feedback control to suppress the undulation of DCB voltage has been prevalently used in practical applications. LADRC classifies all uncertainties acting on the controlled object as "total perturbation", and estimates and compensates for them by the linear extended state observer (LESO) [11]. In addition, the pole configuration method was used to successfully reduce the complex parameter tuning steps, which promoted the application of the LADRC controller in engineering projects [12]. Compared with traditional PI controllers, LADRC's ability to estimate and compensate for uncertain disturbances can make independent PV-storage microgrids have stronger dynamic performance and anti-interference capabilities [13].

Rested on the basis of VCDCC, the second-order LADRC is applied in the voltage loop, and the fuzzy control (FC) is applied to enhance the control accuracy of the system, so as to strengthen the stability and tracing speed of the system to changes in external conditions.

CONSTRUCTION AND OPERATIONAL PRINCIPLE OF INDEPENDENT PHOTOVOLTAIC ENERGY STORAGE SYSTEM

The overall structure of the IPESS appears in Figure 1, and the system is composed of diverse loads, converters, photovoltaic arrays (PV), MPPT circuits, and ESD. The presence of ESD can enhance the operational stability of the entire system. When the PV output electric energy is not less than the prescribed value of the bus, the ESD is in a charging state, and the electric energy is transmitted to the ESD by the DCB for storage. When the PV output power is less than the rated value of the bus demand, the energy stored by the ESD is in turn transmitted to the DCB, so that the system can output power stably.

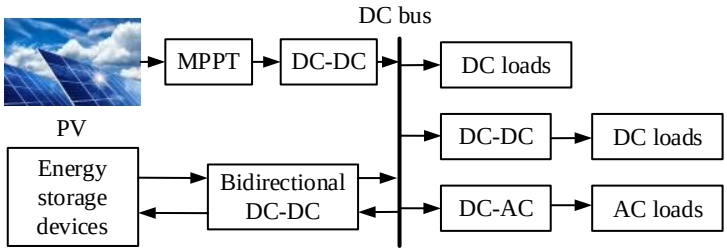

Figure 1. Diagram of the overall structure of IPESS

For the purpose of altering the direction of power transmission between the ESD and the DCB, the BDC needs to track the power change of the system at any time.

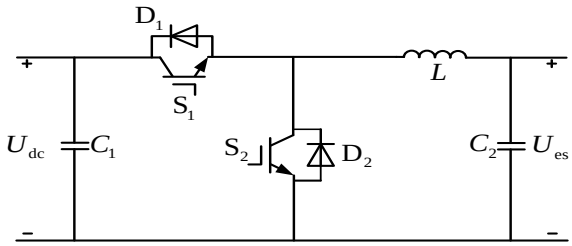

Figure 2. BDC topology

In this paper, a non-isolated BDC converter topology for charging and discharging ESD is applied. It uses two bidirectional switches, such as MOSFETs or IGBTs, to supply the bidirectional power flow necessary for battery charging and discharging, as depicted in Figure 2.

DESIGN OF BDC FOR PHOTOVOLTAIC ENERGY STORAGE

The most important part of the BDC is composed of two diodes D1 and D2 and two switches S1 and S2 in anti-parallel as illustrated in Figure 2. It runs in two modes, Buck-mode and Boost-mode. The BDC circuit in Figure 2 is modeled below. In this modeling, the ideal inductance and capacitance are obtained, and the state variables

are the voltage UC1 of the DCB side capacitor C1, the voltage UC2 of the ESD side capacitor C2, and the inductor current iL, and the DCB voltage Udc and the ESD side Ues are the input disturbances, and the mathematical model of the converter in Buck-mode and Boost-mode is established respectively [14].

The Mathematical Model in Buck-Mode

When the switch S1 is activated and S2 is deactivated, the anti-parallel diodes D1 and D2 are in the cut-off state, and the converter works in Buck-mode, and the corresponding circuit can be seen in Figure 3. From Kirchhoff's theorem, the equation of state of state 1 of the circuit is

$$\begin{cases} \frac{dU_{C1}}{dt} = \frac{1}{R_{dc}C_1}U_{dc} - \frac{1}{C_1}i_L \\ \frac{dU_{C2}}{dt} = -\frac{1}{R_{es}C_2}U_{es} + \frac{1}{C_2}i_L \\ \frac{di_L}{dt} = \frac{1}{L}U_{C1} - \frac{1}{L}U_{C2} \end{cases} \tag{1}$$

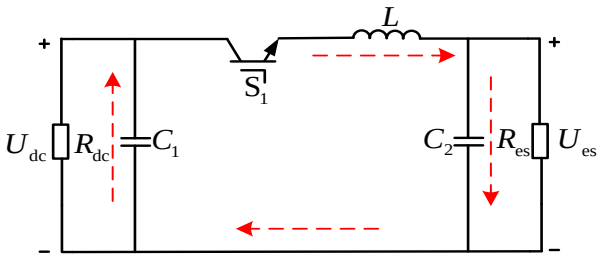

Figure 3. State 1 corresponding circuit in Buck-mode

When the switch tubes S1 and S2 are deactivated, at this time, the anti-parallel diode D1 is in the cut-off state and D2 is in the conduction state, and the corresponding circuit is presented in Figure 4. From Kirchhoff's theorem, the equation of state of state of the circuit at state 2 is

$$\begin{cases} \frac{dU_{C1}}{dt} = \frac{1}{R_{dc}C_1}U_{dc} \\ \frac{dU_{C2}}{dt} = -\frac{1}{R_{es}C_2}U_{es} + \frac{1}{C_2}i_L \\ \frac{di_L}{dt} = -\frac{1}{L}U_{C2} \end{cases} \tag{2}$$

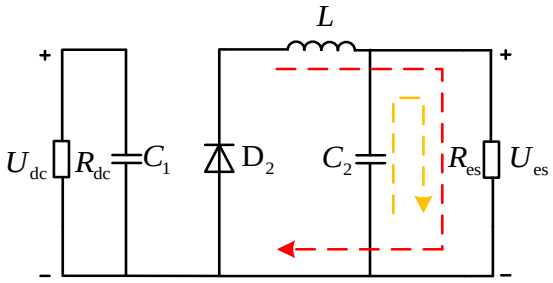

Figure 4. State 2 corresponding circuit in Buck-mode

The state-space average equation when the circuit works in Buck-mode is obtained by the state-space average method, and then the transfer function (TF) when the circuit operates in Buck-mode is obtained by small-signal modeling, as shown in Eq. (3). where dBuck is the duty cycle in Buck-mode; Rdc and Res are the equivalent resistors of the DCB side and the ESD side, respectively.

$$\begin{cases} G_{Ud1}(s) = \frac{U_{es}(s)}{d_{buck}(s)} = \frac{U_{dc}}{LC_2s^2 + L/R_{es}s + 1} \\ G_{id1}(s) = \frac{i_L(s)}{d_{buck}(s)} = \frac{U_{dc}\left(C_2s + 1/R_{es}\right)}{LC_2s^2 + L/R_{es}s + 1} \end{cases} \tag{3}$$

The Mathematical Model in Boost-Mode

The transfer function of the Boost-mode is calculated in the same way as the Buck-mode, and the formula of the TF when the circuit is working in the Boost-mode is depicted in Eq. (4).

$$\begin{cases} G_{Ud2}(s)=\dfrac{U_{dc}(s)}{d_{boost}(s)}=\dfrac{U_{dc}(1-d_{boost})-Li_Ls}{LC_1s^2+L/R_{dc}s+(1-d_{boost})^2} \\ G_{id2}(s)=\dfrac{i_L(s)}{d_{boost}(s)}=\dfrac{U_{dc}\left(C_1s+1/R_{dc}\right)+(1-d_{boost})i_L}{LC_1s^2+L/R_{dc}s+(1-d_{boost})^2} \end{cases} \tag{4}$$

FS-LDARC CONTROL STRATEGY

The second-order LADRC block of the voltage loop is displayed in Figure 5. Uref is the reference value of the DCB voltage; b0 is the control gain; u is the control quantity; z1 is the real-tim voltagee of the DCB; z2 is the differentiation of the real-time DCB voltage; z3 is the total perturbation.

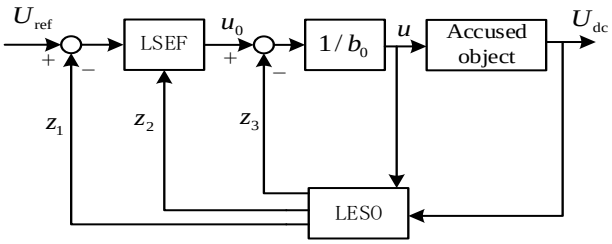

Figure 5. Block diagram of the second-order LADRC of a voltage loop

The traditional active disturbance rejection controller has a relatively low parameter adjustment accuracy, which results in the deterioration of control performance, and the system control accuracy is low under complex conditions. However, there is no correlation between the FC algorithm and the mathematical model of the controlled object, and the control parameters can be dynamic, which makes the parameter adjustment more fine, thus enhancing the control precision of the system [15]. Therefore, on the basis of the VCDCC structure, the control mode combining FC and second-order LADRC method is adopted on the voltage loop to optimize the control effect of the system.

The current loop is controlled by PI, and the control block diagram is visualized in Figure 6. Among them, Hv(s) and Hi(s) are the TF of the voltage loop and the current loop sampling link, Gm(s) is the TF of the modulation link, Gid(s) is the TF of the inductor current to duty cycle, and Gvi(s) is the TF of the DCB voltage to the inductor current.

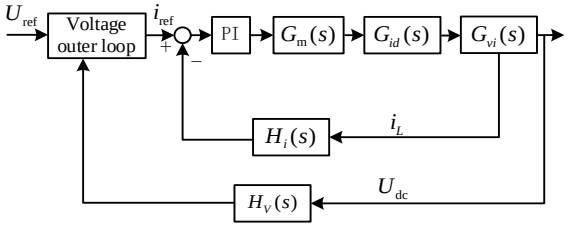

Figure 6. Diagram of the current inner loop control block

Second-Order LADRC Design

The second-order LADRC can transform the controlled object into an integrator series system through the disturbance compensation link, simplifying the parameter adjustment link. The controlled object of the second-order LADRC is determined as

$$\ddot{y} = bu + f(y, \dot{y}, \omega, t) \tag{5}$$

where y, u, ω, f are the output, input, external perturbation, and total perturbation, respectively. Eq. (5) can be rewritten as:

$$\ddot{y} = b_0 u + (b - b_0)u + f(y, \dot{y}, \omega, t) \tag{6}$$

Calculate (b-b0) u into the external perturbation ω

$$\ddot{y} = b_0 u + f(y, \dot{y}, \omega, t) \tag{7}$$

Select the state variable, ie

$$\begin{cases} x_1 = y \\ x_2 = \dot{y} \\ x_3 = f \\ h = \dot{f} \end{cases} \tag{8}$$

Eq. (8) can be transformed into a continuously expanding equation of state of Eq. (9), ie

$$\begin{cases} \dot{x}_1 = x_2 \\ \dot{x}_2 = x_3 + bu \\ \dot{x}_3 = h \\ y = x_1 \end{cases} \tag{9}$$

According to Luenberger's state observer theory, the equation for the Continuous Linear State Observer (LESO) corresponding to Eq. (8) is

$$\begin{cases} \dot{z}_1 = \beta_1(y - z_1) + z_2 \\ \dot{z}_2 = \beta_2(y - z_1) + z_3 + b_0 u \\ \dot{z}_3 = \beta_3(y - z_1) \end{cases} \tag{10}$$

β1, β2, β3 are observer gains, and if ω0 (observer gain) is selected, LESO can track the state variables of the controlled object. The observation and tracking performance of LESO directly affects the control performance of LADRC. For the Laplace transformation of the LESO equation, the characteristic equation of LESO is obtained

$$\lambda(s) = s^3 + \beta_1 s^2 + \beta_2 s + \beta_3 \tag{11}$$

The bandwidth method (ω0 is the observer bandwidth, kp=ωc2, kp=2ωc, ωc is the controller bandwidth), order

$$\lambda(s) = (s + \omega_0)^3 \tag{12}$$

Available

$$\beta_1 = 3\omega_0, \beta_2 = 3{\omega_0}^2, \beta_2 = {\omega_0}^3 \tag{13}$$

Simplification of the system, ordering

$$u = \frac{(u_0 - z_3)}{b_0} \tag{14}$$

The system can be simplified to a two-integrator series system, i.e

$$\ddot{y} = u_0 \tag{15}$$

It can be obtained by designing the integrator series system LSEF

$$u_0 = k_p(U_{\text{ref}} - z_1) - k_d z_2 \tag{16}$$

where Uref is the given signal and kp and kd are the controller gains.

Fuzzy LADRC Design

Compared with the traditional PI and the traditional first-order LADRC, the second-order LADRC controller has a better ability to eliminate system errors. Due to the complexity and limitations of stand-alone PV energy storage systems, traditional control theories have strong control capabilities for explicit systems, but are powerless for

systems that are too complex or difficult to describe accurately. Therefore, fuzzy mathematics is used to deal with these control problems, and FC technology can make up for the shortcomings of traditional control technology with inaccurate processing and high uncertainty of control, and possesses remarkable advantages when dealing with large and highly intricate systems. The control method combining FC and second-order LADRC can effectively improve the stability of the system and improve the tracking performance of DCB voltage, and the structure of FS-LADRC is represented in Figure 7.

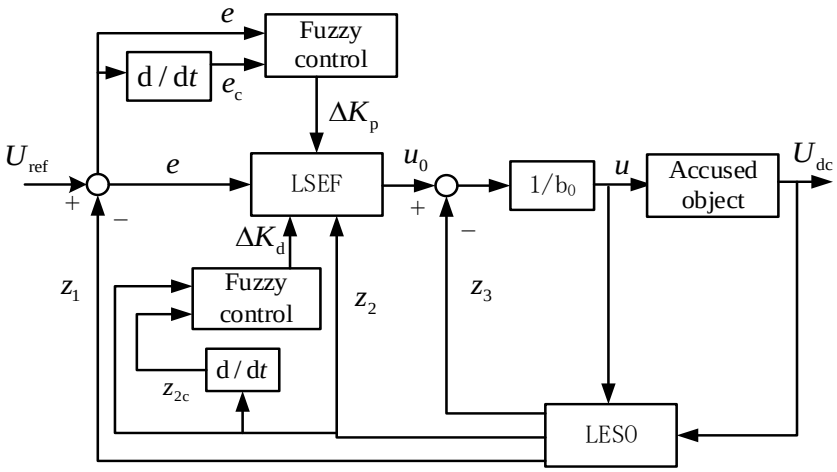

Figure 7. FS-LADRC control block diagram

The controller takes the error e of DCB voltage and its differential ec as input variable, and the output variable is Δkp, the differential z2 of DCB voltage and its differentiation z2c as input variable, and the output variable is Δkd, utilizes the characteristics of second-order LADRC, respectively, carries out FC of the disturbance of DCB voltage and the differentiation of DCB voltage, because Δkp and Δkd use two FC to adjust respectively, can make controller parameter setting more accurate and improve the control accuracy of controller, The parameters adjusted by the FC are:

$$\begin{cases} k_{p1} = \Delta k_p + k_{p1} \\ k_{d1} = \Delta k_d + k_{d1} \end{cases} \tag{17}$$

kp1 and kd1 are the feedback error gains of the improved LADRC, and the system LSEF equation is

$$u_0 = k_{p1}(U_{\text{ref}} - z_1) - k_{d1} z_2 \tag{18}$$

Through theoretical analysis, it is determined that the DCB voltage error e and its differential ec, the differential of DCB voltage and the fuzzy subset domain of its differential are [-3,3], [-5,5], [-5,5], [-8,8], respectively, and the fuzzy subset domain of Δkp is [-8,8], and the fuzzy subset domain of Δkd is [-10,10], then their fuzzy subsets can be {NB,NM,NS,ZO,PS,PM,PB}, which represent negative large, negative medium, negative small, and zero, respectively, is small, is in the middle, is large. Through the analysis of the characteristics of the independent photovoltaic storage and power generation system, the triangle is used as the input and output membership functions. According to the theoretical analysis, the rules table of the FC are represented in Tables 1 and 2.

Table 1. Δkp FC rule table

$e\backslash e_c$	NB	NM	NS	ZO	PS	PM	PB
NB	PB	PB	PM	PM	PS	ZO	ZO
NM	PB	PB	PM	PS	PS	ZO	NS
NS	PM	PM	PS	PS	NS	NM	NB
ZO	PM	PM	PS	ZO	NS	NM	NM
PS	PS	PS	ZO	NS	NS	NM	NB
PM	PS	ZO	NS	NM	NM	NM	NB
PB	ZO	ZO	NM	NM	NS	NB	NB

Table 2. Δkd FC rule table

$z_2 \backslash z_{2c}$	NB	NM	NS	ZO	PS	PM	PB
NB	PB	PB	PS	PM	PS	ZO	ZO
NM	PB	PM	PM	PS	PS	ZO	NS
NS	PB	PM	PS	PS	NS	NS	NS
ZO	PB	PM	PS	ZO	NS	NM	NM
PS	PB	PM	PS	NS	NS	NM	NM
PM	PS	ZO	NS	NM	NM	NM	NB
PB	ZO	ZO	NM	NM	NM	NB	NB

SIMULATION ANALYSIS

For the sake of validating the effect and performance of the FS-LADRC in the research system in this paper, a distributed photovoltaic energy storage small signal model was built through the Simulink simulation platform, and the main parameters of the design model are depicted in Table 3.

Table 3. Simulate some of the parameters

The name of the parameter	numeric value
DC bus voltage$/V$	220
Load resistance$/\Omega$	50
inductance$L/$mH	2
capacitance$C_1/\mu F$	450
capacitance$C_2/\mu F$	550
Compensate for the gainb_0	9.65×10^5
Controller bandwidthω_c	1850
Observer bandwidthω_0	830
Switching frequencyf_S/H	10^4

In order to verify the feasibility of FS-LADRC in an independent optical storage system, the three control methods were analyzed under constant conditions (temperature 25℃; irradiance 1000W/m2) during start-up and stable operation. The irradiance variation is exhibited in Figure 8.

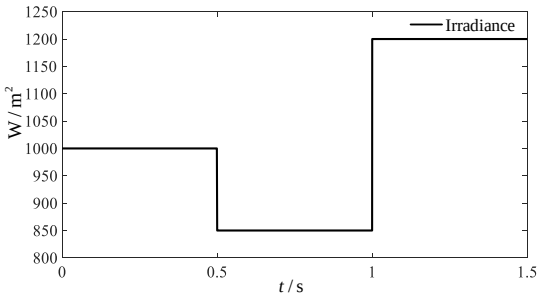

Figure 8. Irradiance change plot

When the total length of the simulation time is 1.5s and t=0-0.5s, the irradiance is 1000W/m2. The temperature is constant at 25℃, the illuminance is reduced to 850W/m2 at 0.5s, lasts until 1s, and then increases the irradiance to 1200W/m2 until the end of 1.5s. First, the start-up process under constant conditions is analyzed for the performance of the three control modes, and the simulation is exhibited in Figure 9.

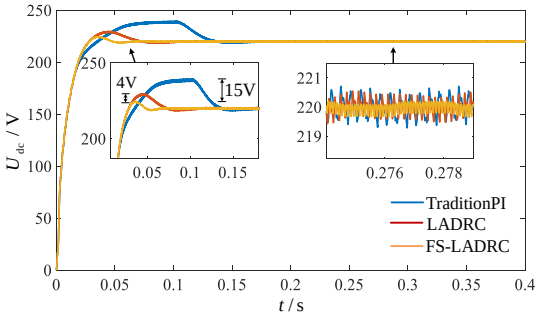

Figure 9. Start-up process DCB voltage waveform under constant conditions

As can be depicted from Figure 9, the FS-LADRC control mode is 15V lower than the traditional PI control overshoot, 4V lower than the traditional LADRC control overshoot, and the adjustment time is 0.08s and 0.02s faster than the traditional PI and traditional LADRC, respectively. The combination of FC and second-order LADRC makes the system parameters more accurate, so that the system has higher control accuracy, and the stability and anti-interference ability of the system are also improved.

Fig. 10 is a comparison diagram of the DCB voltage under the condition of changing the irradiance of each control mode in stable operation, the illumination suddenly drops from 1000W/m2 to 850W/m2 at 0.5s, at this time, the light is insufficient, the DCB voltage does not reach the rated value, the battery is discharged, and the BDC is in Boost- mode.

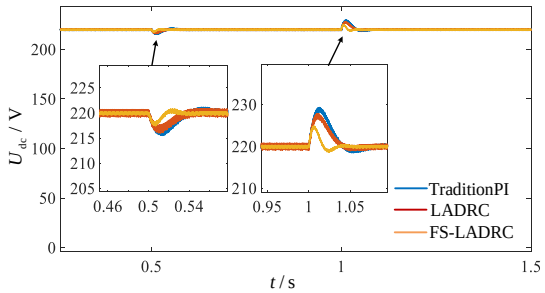

Figure 10. Irradiance change DCB voltage waveform

At 1s, the irradiance drops from 850W/m2 to 1200W/m2, at this time, the light is too strong, the DCB voltage will be greater than the rated value, the ESD is in the charging state, the BDC is in Buck-mode, and the electric energy is transmitted to the ESD by the DCB for storage.

Table 4 shows the comparison of the data of the three control strategies under different conditions.

Table 4 Comparison of the performance of different control strategies

Tactics	Constant conditions		Sudden decrease in irradiance		Sudden increase in irradiance	
	Adjustment time(s)	Overshoot (V)	Adjustment time(s)	Overshoot (V)	Adjustment time(s)	Overshoot (V)
FS-LADRC	0.06	4	0.02	2.3	0.03	4.6
LADRC	0.08	8	0.037	3.5	0.04	7.5
PI	0.14	19	0.04	3.8	0.05	8.8

CONCLUSIONS

For the purpose of tackling the problem of power supply reliability of independent photovoltaic energy storage system, this paper proposes a control method combining FC and second-order LADRC to control the BDC connecting the independent photovoltaic system and the energy storage system. The system simulation model was established by MATLAB/simulink software, and the energy storage BDC was compared with FS-LADRC, traditional LADRC and traditional PI control. Through the analysis of the DCB voltage waveform during the start-

up process and the stable operation process under constant conditions, it is concluded that the voltage overshoot, ripple size and tracking speed of FS-LADRC in the three processes are better than the other two control methods, and the robustness and anti-interference ability of the system are enhanced, and the power supply reliability of the system is improved.

ACKNOWLEDGMENTS

This work was supported by the Natural Science Foundation of Hunan Province (2022JJ50111), Xiangtan Science and Technology Project (CG-YB20221045) and Hunan Provincial Graduate Research and Innovation Project Funding (YC202319).

REFERENCES

[1] Ma H F. Analysis on the status quo and development of solar photovoltaic power generation technology. Light Source & Lighting, 2023, (09):114-116.

[2] Javaid N, Hafeez G, Iqbal S, et al. Energy Efficient Integration of RenewableEnergy Sources in the Smart Grid for Demand Side Management. IEEE Access 2018, 6, 77077-77096.

[3] Xue J X, Cai D L, Jin L. Design of bidirectional DC-DC photovoltaic energy storage loop based on LLC resonant converter. Automation and instrumentation2024, 39(02):11-15. DOI: 10.19557/j.cnki.1001-9944.2024.02.003.

[4] Hussain A, Akhtar R, Ali B, et al. A novel bidirectional DC-DC converter with low stress and low magnitude ripples for stand-alone photovoltaic power systems. Energies, 2019, 12(15):2884.

[5] Yaseen M, Farooq A, Malik M Z, et al. Design of a High Step-Up DC-DC Converter with Voltage Doubler and Tripler Circuits for Photovoltaic Systems. Int. J. Photoenergy 2021, 2021, 1-11.

[6] Li B, Li L, Wang H, et al. A droop control for improving load current distribution in DC microgrid. Journal of Electric Power Science and Technology, 2022, 37(01):48-54. DOI: 10.19781/j.issn.1673-9140.2022.01.006.

[7] Liu S, Liu X, Jiang S, et al. Application of an Improved STSMC Method to the Bidirectional DC-DC Converter in Photovoltaic DC Microgrid. Energies, 2022, 15(5):1636.

[8] Wu Y E, Hong R R. Multi-Functional Isolated Three-Port Bidirectional DC/DC Converter for Photovoltaic Systems. Sustainability, 2022, 14(18):11169.

[9] Wang M, Tian Y, Li T M, et al. Research on bidirectional DC-DC converter applied to energy storage system. Transactions of China Electrotechnical Society, 2013, 28(08):66-71. DOI: 10.19595/j.cnki.1000-6753.tces.2013.08.009.

[10] Huang L, Wang P, Wu J W, et al. Bidirectional DC-DC nonlinear control of distributed photolar-storage power generation system. Transactions of China Electrotechnical Society, 2016, 31(S2):10-18. DOI: 10.19595/j.cnki.1000-6753.tces.2016.s2.002.

[11] Huang Y, Xue W C. Active disturbance rejection control: methodology and theoretical analysis. Isa Transactions, 2014, 53(4):963-976.

[12] Gao Z Q. Research on the Idea of Active Disturbance Rejection Control. Control Theory and Applications, 2013, 30(12): 1498-1510.

[13] Yang H, Luo S, Sun X D, et al. Research on active disturbance rejection control method of bidirectional DC-DC converter for photovoltaic energy storage. Acta Solaria Sinica, 2018, 39(05):1342-1350. DOI: 10.19912/j.0254-0096.2018.05.024.

[14] Elserougi A A, Massoud A M, Ahmed S. A unipolar/bipolar high-voltage pulse generator based on positive and negative Buck-Boost DC-DC Converters operating in discontinuous conduction mode. IEEE Trans. Ind. Electron. 64(7), 5368-5379 (2017)

[15] Dou Q B, Wang H L, Pi D W, et al. Research on yaw stability control of intelligent vehicles fusing LSTM and fuzzy control. Agricultural Equipment and Vehicle Engineering, 2023, 61(12):69-74.